Electronic Supplementary Material (ESI) for Journal of Materials Chemistry A.

Electronic Supporting Information

Porous gC_3N_4-$Gd_2Zr_2O_7$ enables the high-temperature operation of Nafion membrane in polymer electrolyte fuel cell over 500 hours

Mohanraj Vinothkannan[a], Byungrak Son[b], and Sangaraju Shanmugam[a,*]

[a] Department of Energy Science and Engineering,

Daegu Gyeongbuk Institute of Science & Technology (DGIST),

50-1, Sang-Ri, Hyeonpung-Myeon, Dalseong-Gun, Daegu 42988, The Republic of Korea.

[b] Division of Energy Technology, Daegu Gyeongbuk Institute of Science & Technology (DGIST), 50-1, Sang-Ri, Hyeonpung-Myeon, Dalseong-Gun, Daegu 42988, Republic of Korea

*E-mail: sangarajus@dgist.ac.kr

Measurements

Water uptake and swelling degree

Water uptake and swelling degree

The test protocols of changes in mass, length, width, and thickness of membranes after water uptake were as follows. The membranes were dried at 90 °C for 12 h in a vacuum oven. The mass (M_{dry}), length (L_{dry}), width (W_{dry}), and thickness (T_{dry}) of the dry membranes were recorded. Next, the membranes were drenched in DI water at 80 °C for 24 h to make them fully absorb water. The excess water on the membrane surfaces was wiped off quickly, and the mass (M_{wet}), length (L_{wet}), width (W_{wet}), and thickness (T_{wet}) were measured again.[1, 2] The water uptake, dimensional change, and thickness change were calculated by the following formulas, respectively.

$$Water\ uptake\ (\%) = \left[\frac{M_{wet} - M_{dry}}{M_{dry}}\right] \times 100 \qquad (S1)$$

$$Dimensional\ change\ (\%) = \left[\frac{(W_{wet} \times L_{wet}) - (W_{dry} \times L_{dry})}{(W_{dry} \times L_{dry})}\right] \times 100 \qquad (S2)$$

$$Thickness\ change\ (\%) = \left[\frac{T_{wet} - T_{dry}}{T_{dry}}\right] \times 100 \qquad (S3)$$

Ion exchange capacity

To quantify the ion exchange capacity (IEC) values of the membranes, dry samples were engulfed into aqueous NaCl (3 M) for 24 h, followed by titration with a NaOH (0.01 M) with a phenolphthalein indicator.[3] The IEC was calculated from the following formula (4).

$$IEC\ (meq.\ g^{-1}) = \frac{Volume\ of\ NaOH\ consumed \times Concentration\ of\ NaOH}{Weight\ of\ dry\ sample} \qquad (S4)$$

Hydration number

The amount of water adsorbed per unit volume of the membrane was estimated by normalizing water uptake capacity with IEC values using the formula (5).[4, 5]

$$Hydration\ number\ (\lambda) = \left[\frac{Water\ uptake}{18.01}\right]\left[\frac{10}{IEC}\right] \qquad (S5)$$

where 18.01 is known as the molecular weight of water (g mol^{-1}).

Oxidative stability

Oxidative stability of the membranes was determined by recording the changes in weight of membranes after treatment in Fenton's reagent (3% H_2O_2 containing 3 ppm $FeSO_4$) at 80 °C for 24 h.[6, 7] The oxidative stability for weight difference can be evaluated by the following formula (6).

$$Oxidative\ stability\ (\%) = \frac{W_{after}}{W_{before}} \times 100 \qquad (S6)$$

Proton conductivity

The proton conductivity of the membrane samples was determined using the alternating-current (AC) impedance method with a conductivity test Bench (Scitech, South Korea). The membrane samples were fixed in four probe Bekk-Tech cells, and the conductivity was measured as a function of temperature. During the measurement, the RH was fixed at 100, 30, or 15 %, and the temperature was varied from 30 to 120 °C, and kept constant for 120 min at each temperature to attain a steady-state.[8, 9] The proton conductivity of the samples was calculated from the following equation (7).

$$\sigma\ (mS\ cm^{-1}) = \frac{L}{RTW} \qquad (S7)$$

where L (0.42 cm fixed), T (cm), W (cm), and R (Ω) are the sample's length, thickness, area, and ohmic resistance, respectively.

Membrane electrode assembly preparation and PEFC test

The routine brush coating method was used to prepare membrane electrode assembly (MEA), as reported in the literature.[2, 10, 11] Catalyst coated carbon papers with a Pt loading of 0.5 mg cm^{-2} were used as the anode and cathode for the MEA. A membrane sample and two pieces of carbon papers were assembled as a sandwich to fabricate the MEA. The hot-compaction was conducted on a lamination jig (Model: HMM-04A) with a load of 20 Kg cm^{-2} at 120 ˚C for 2 min. Next, the MEA was coupled with Teflon gaskets and fixed at the single cell equipped with a bipolar plate with a serpentine flow field machined on graphite plates (active area: 5 cm^2). Then, the end plates of single cells were firmly assembled by fastening bolts with a torque of 38 N m. The PEFC test was performed at 80, 100, or 125 ˚C under 100, 30, or 15% RH, respectively, without applying anode and cathode back-pressure using Scribner fuel cell test system (model: 850e Multi Range). The PEFC performance was measured for two specimens per membrane to confirm reproducibility. To evaluate the durability of membrane specimens, open-circuit voltage (OCV) decay was monitored as a function of time at 100 ˚C under 30% RH. On the other side, the fluoride ion (F^-) concentration in the outlet liquids from anode and cathode outlets was also quantified during the OCV decay test at 100 ˚C under 30% RH using a fluoride-ion-selective electrode (Thermo Scientific, Orion 9009061). The outlet liquids were collected for each 20 h interval.

Hydrogen permeability

The hydrogen permeability across the membranes has been evaluated in the PEFC (at 100 ˚C under 30% RH) configuration by linear sweep voltammetry (LSV) with a scan rate of 2 mV s^{-1} in a sweep range of 0 to 0.6 V using a potentiostat (model: 885 Fuel Cell Potentiostat). During the measurement, the anode was kept under hydrogen purge (300 mL min^{-1}) as the reference electrode, and the cathode was kept under nitrogen purge (300 mL min^{-1}) as the working electrode. The crossover hydrogen from the anode to cathode oxidize at the cathode and deliver the current is represented as hydrogen crossover current. Hydrogen crossover flux (mol cm^{-2} s^{-1}) across membranes was calculated using Faraday's equation (8).

$$J_{flux} = \frac{i_{lim}}{(nF)} \qquad (S8)$$

where i_{lim} is limiting current derived from LSV, n is number of electrons involved in reaction and F is Faraday constant.

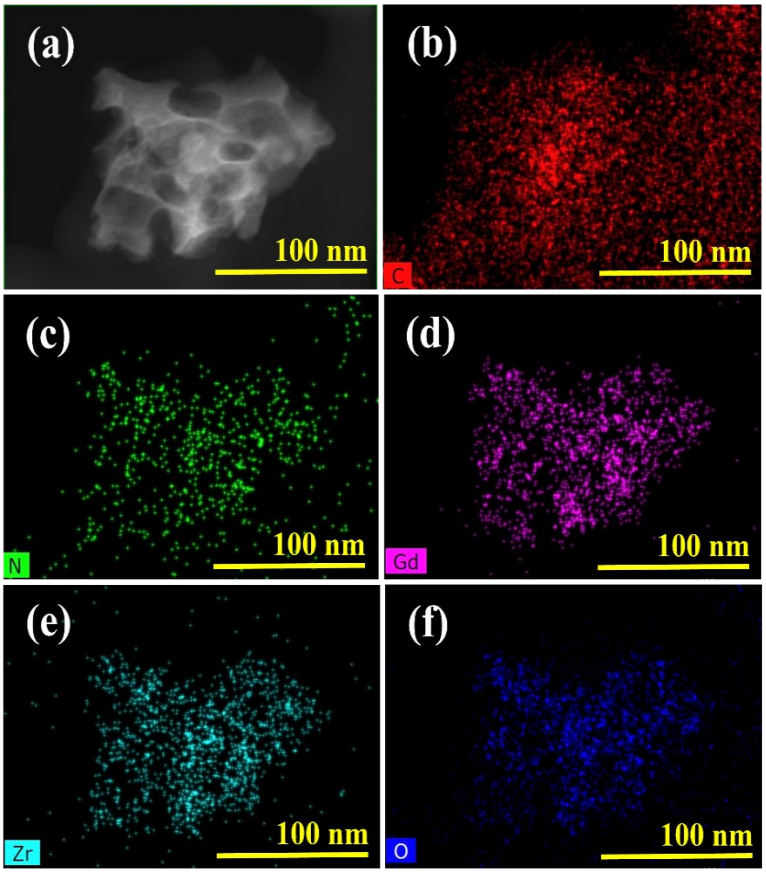

Fig. S1. FETEM elemental mappings of gC_3N_4-$Gd_2Zr_2O_7$ correspond to (a) bright field image, (b) C-K, (c) N-K, (d) Gd-L, (e) Zr-L, and (f) O-K.

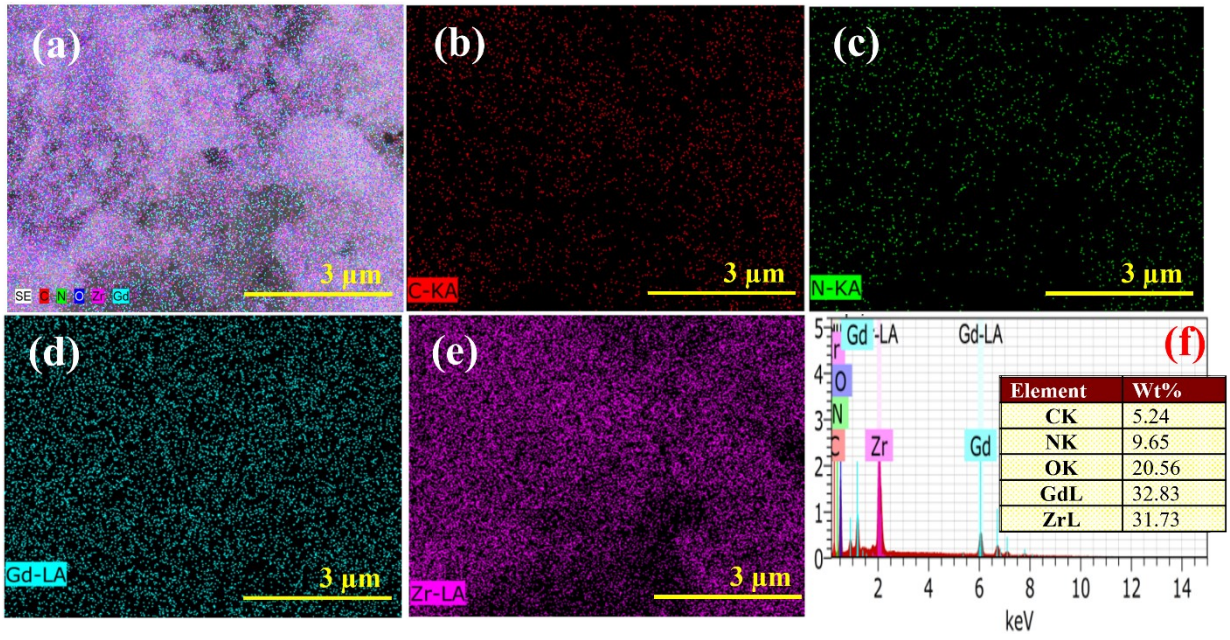

Fig. S2. SEM elemental mappings of gC_3N_4-$Gd_2Zr_2O_7$ with respect to (a) overlapping of elements, (b) C-K, (c) N-K, (d) Gd-L, and (e) Zr-L; (f) EDS spectra of gC_3N_4-$Gd_2Zr_2O_7$.

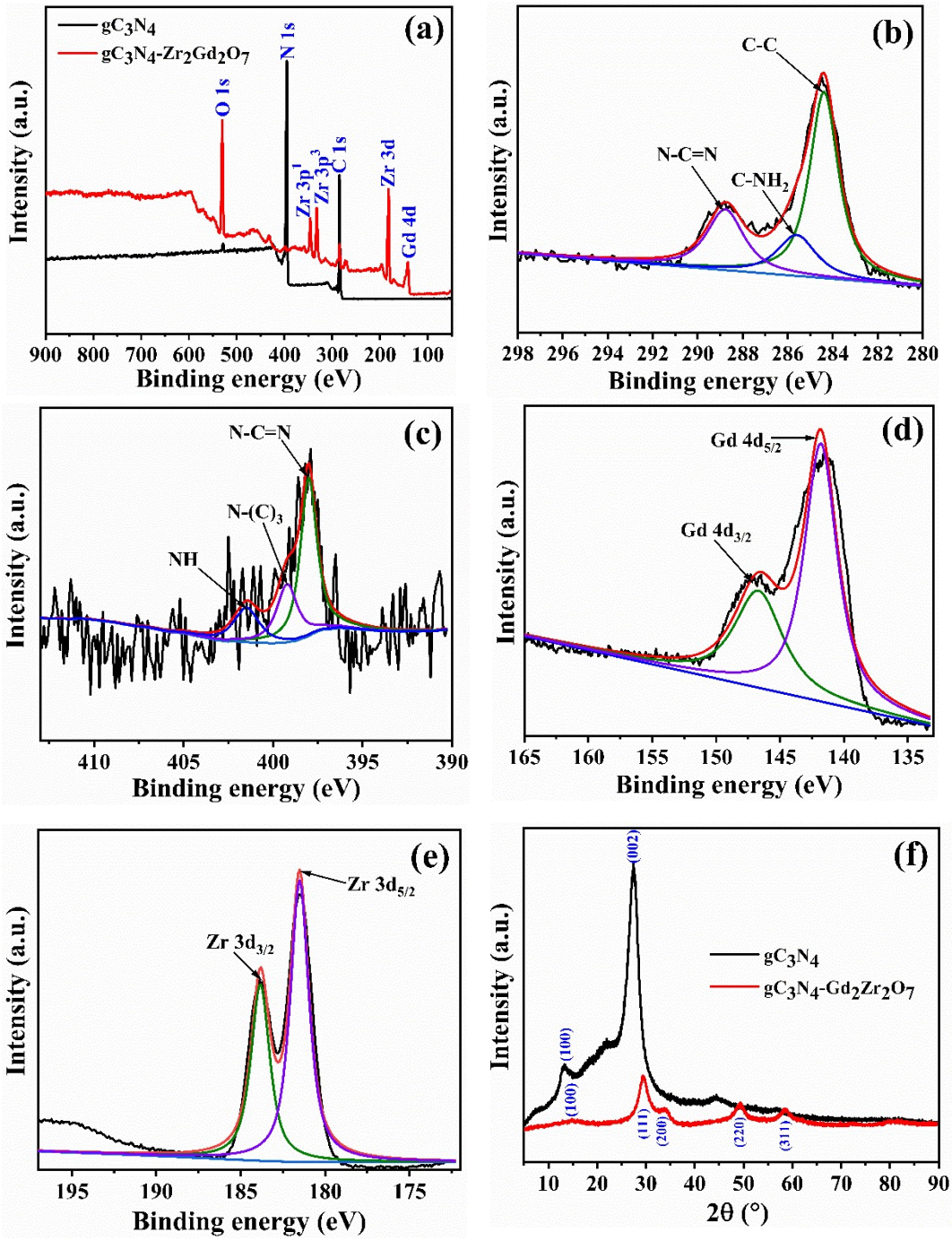

Fig. S3. XPS analysis of pristine gC_3N_4 and gC_3N_4-$Gd_2Zr_2O_7$: (a) survey spectrum, (b) C 1s, (c) N 1s, (d) Gd 4d, and (e) Zr 3d; (f) XRD patterns of pristine gC_3N_4 and gC_3N_4-$Gd_2Zr_2O_7$.

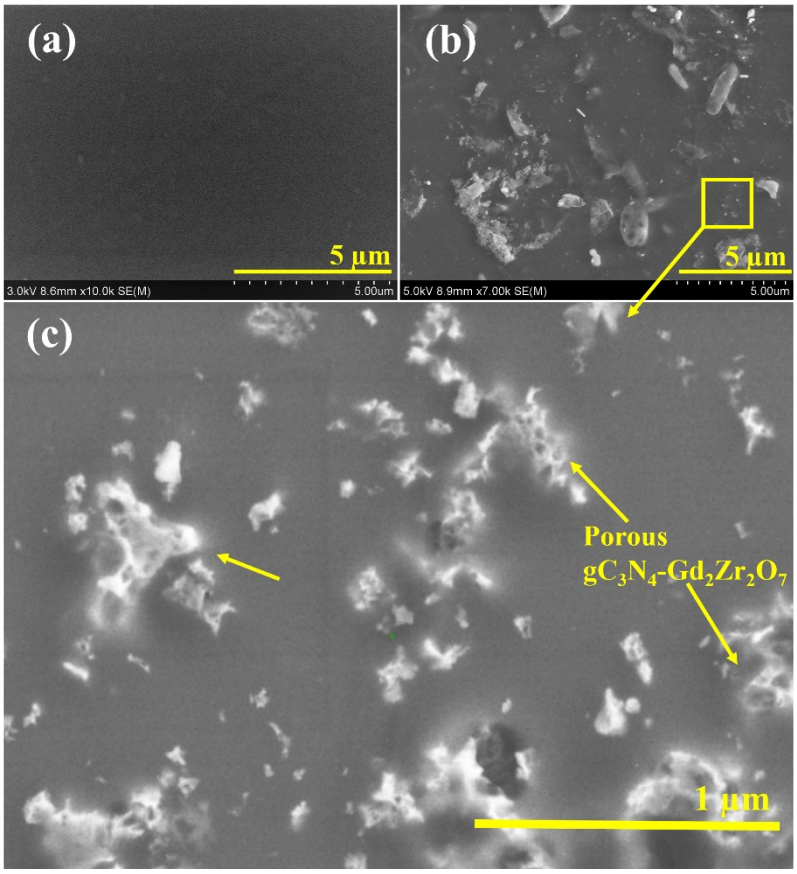

Fig. S4. SEM images correspond to the top-view morphology of (a) pristine Nafion and (b and c) Nafion/gC_3N_4-$Gd_2Zr_2O_7$.

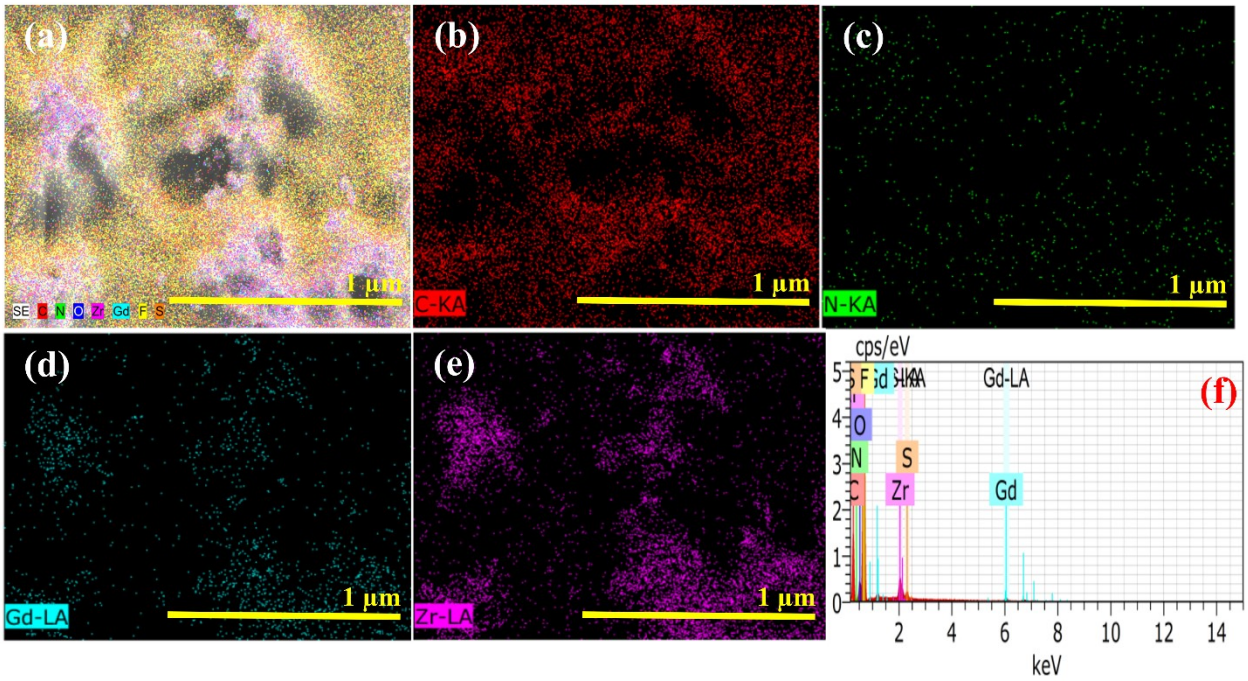

Fig. S5. SEM elemental mappings of Nafion/gC_3N_4-$Gd_2Zr_2O_7$ with respect to (a) overlapping of elements, (b) C-K, (c) N-K, (d) Gd-L, and (e) Zr-L; (f) EDS spectra of Nafion/gC_3N_4-$Gd_2Zr_2O_7$.

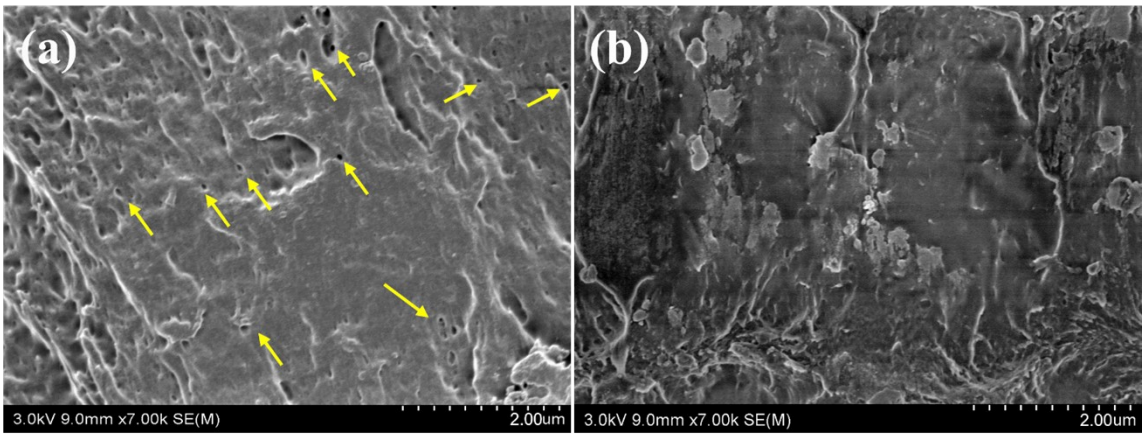

Fig. S6. SEM images correspond to the cross-sectional morphology of (a) pristine Nafion and (b) Nafion/gC_3N_4-$Gd_2Zr_2O_7$.

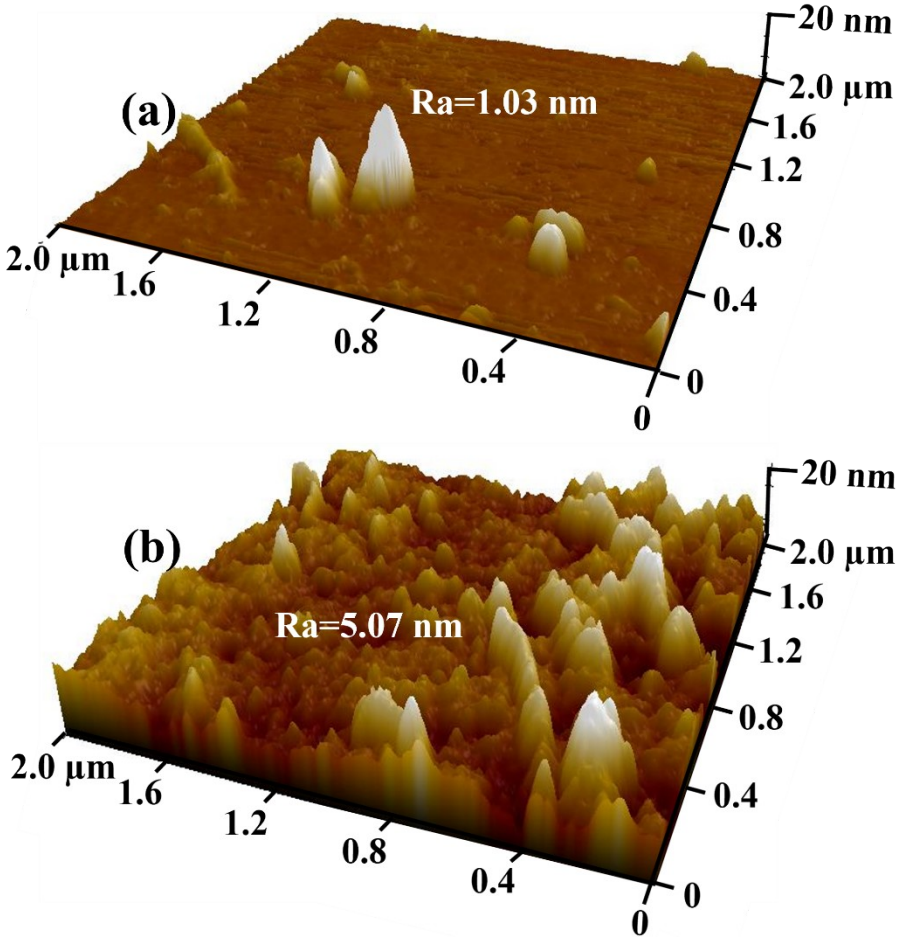

Fig. S7. AFM height images of (a) pristine Nafion and (b) Nafion/gC_3N_4-$Gd_2Zr_2O_7$.

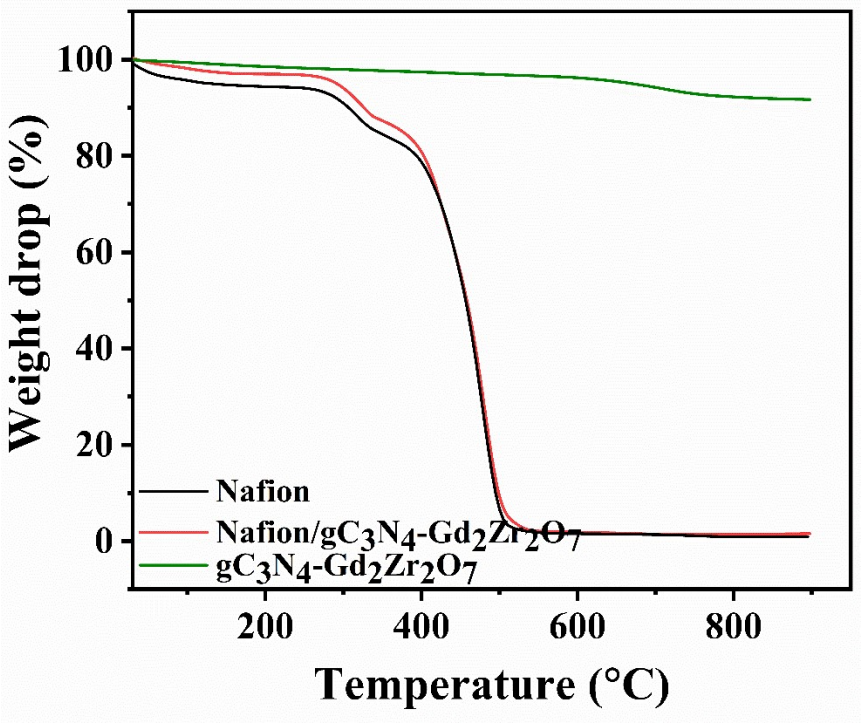

Fig. S8. TGA curves of pristine Nafion and Nafion/gC_3N_4-$Gd_2Zr_2O_7$.

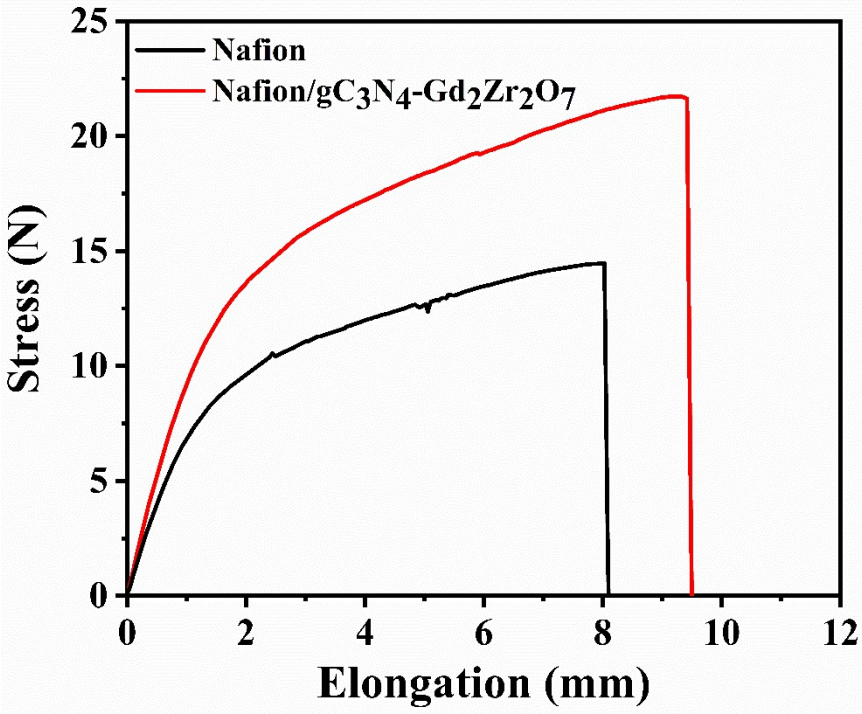

Fig. S9. UTM curves of pristine Nafion and Nafion/gC_3N_4-$Gd_2Zr_2O_7$.

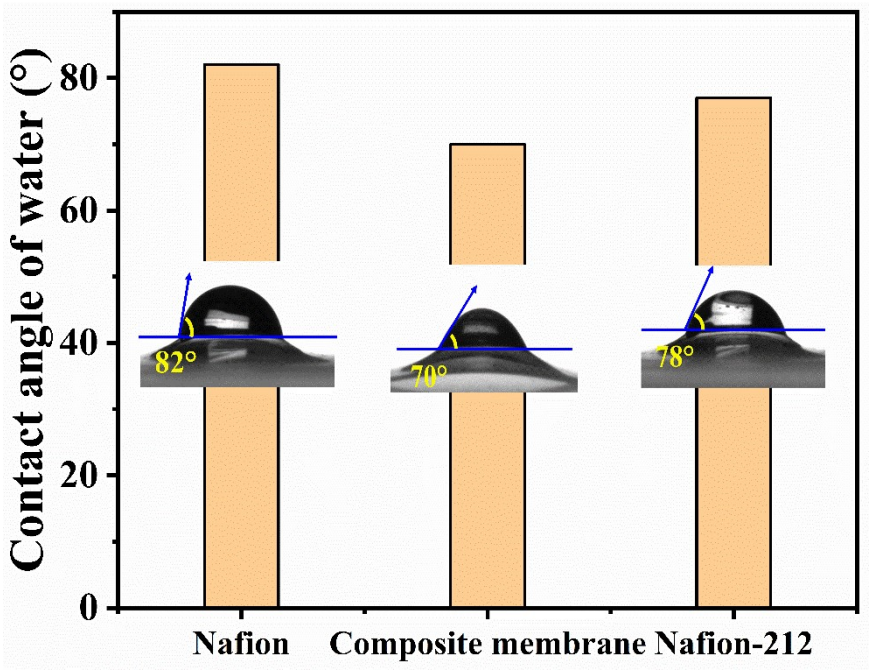

Fig. S10. Contact angle of water on prepared membranes quantified at room temperature.

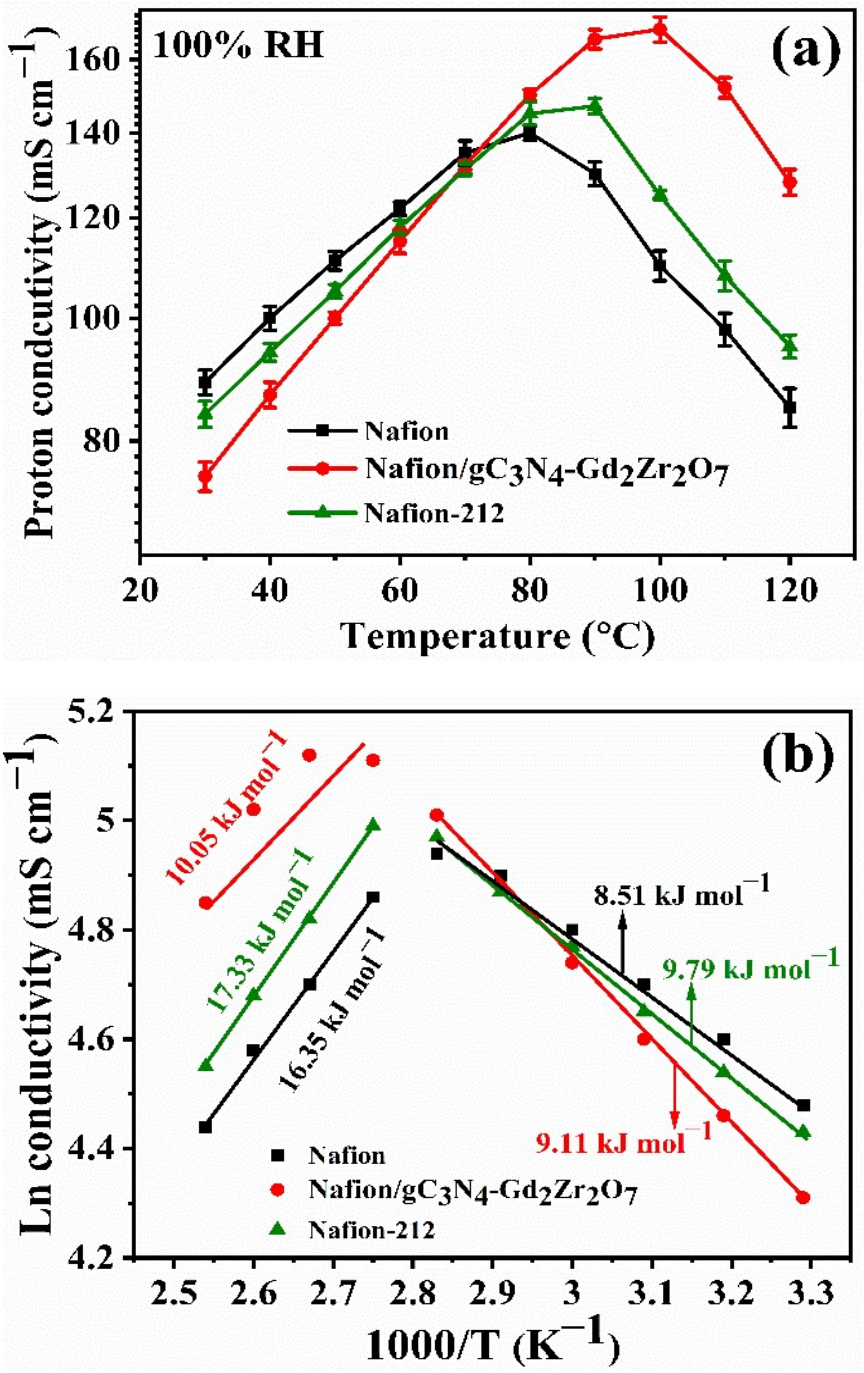

Fig. S11. (a) Proton conductivity plots of pristine Nafion, Nafion-212, and composite membranes as a function of temperature at 100% RH and (b) corresponding Arrhenius plots derived from proton conductivities.

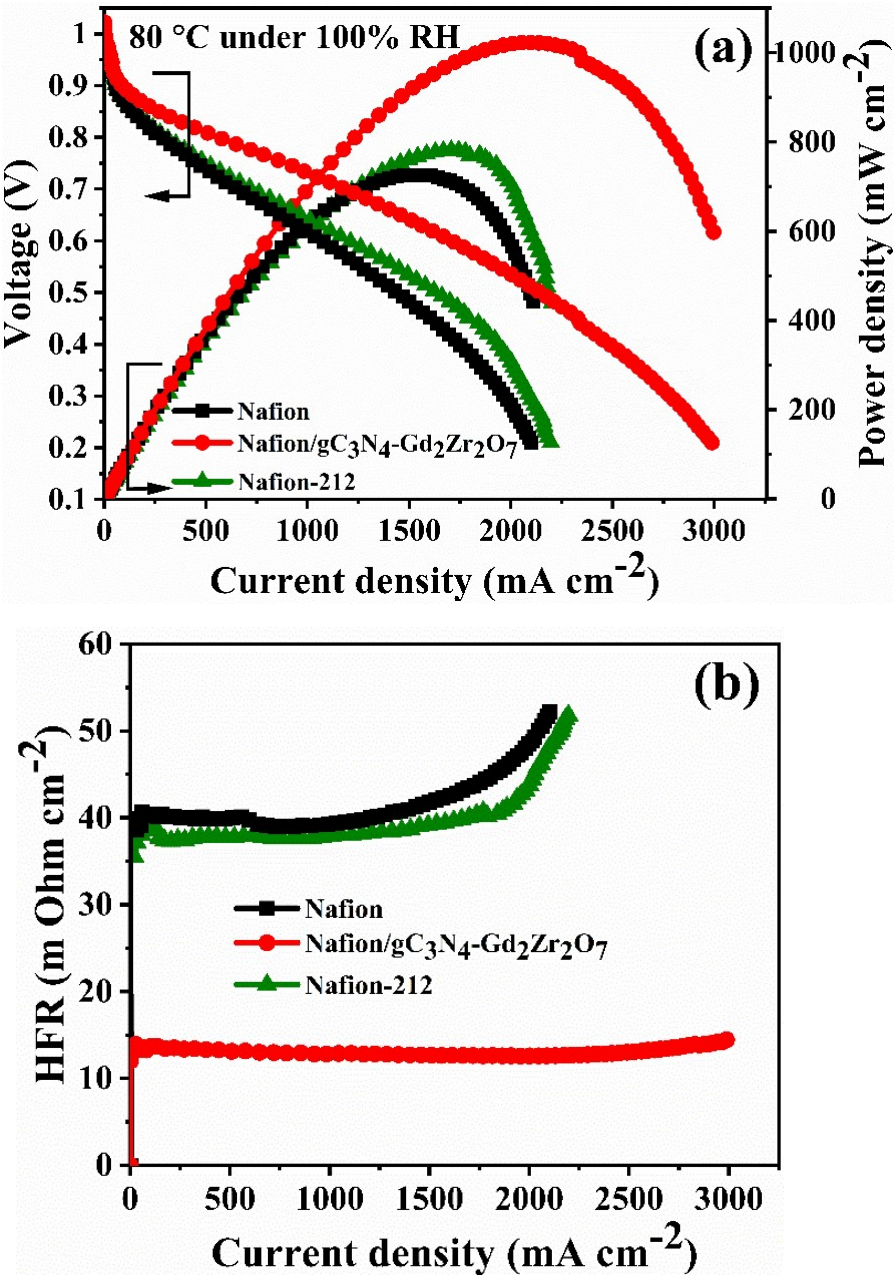

Fig. S12. (a) PEFC polarization curves and (b) high-frequency resistance (HFR) curves of pristine Nafion, Nafion-212, and composite membranes quantified at 80 °C under 100% RH.

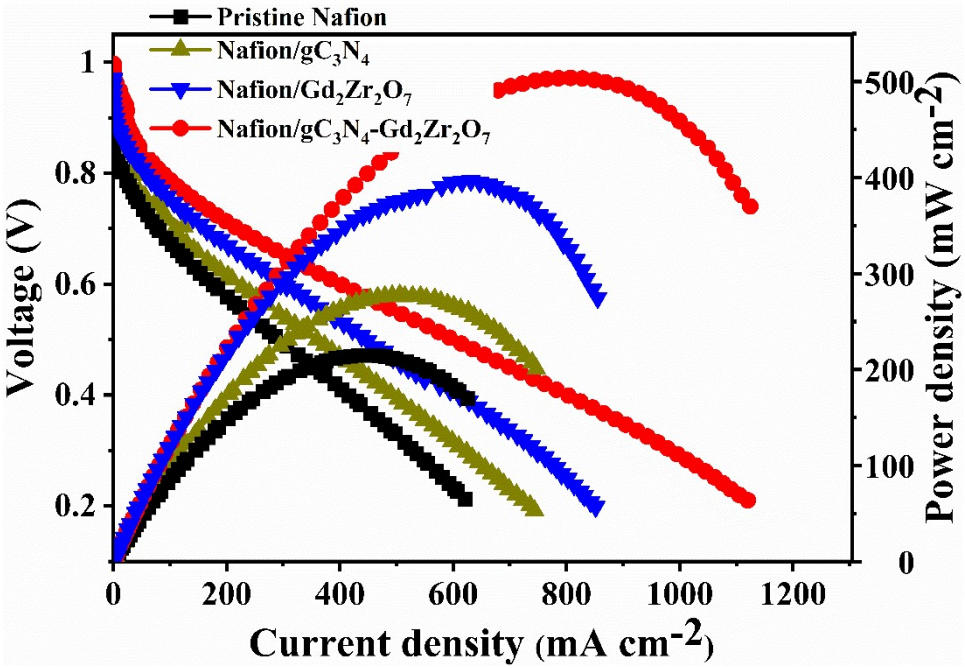

Fig. S13. PEFC polarization curves of pristine Nafion, Nafion/gC_3N_4, Nafion/$Gd_2Zr_2O_7$, and Nafion/gC_3N_4-$Gd_2Zr_2O_7$ membranes quantified at 100 °C under 30% RH.

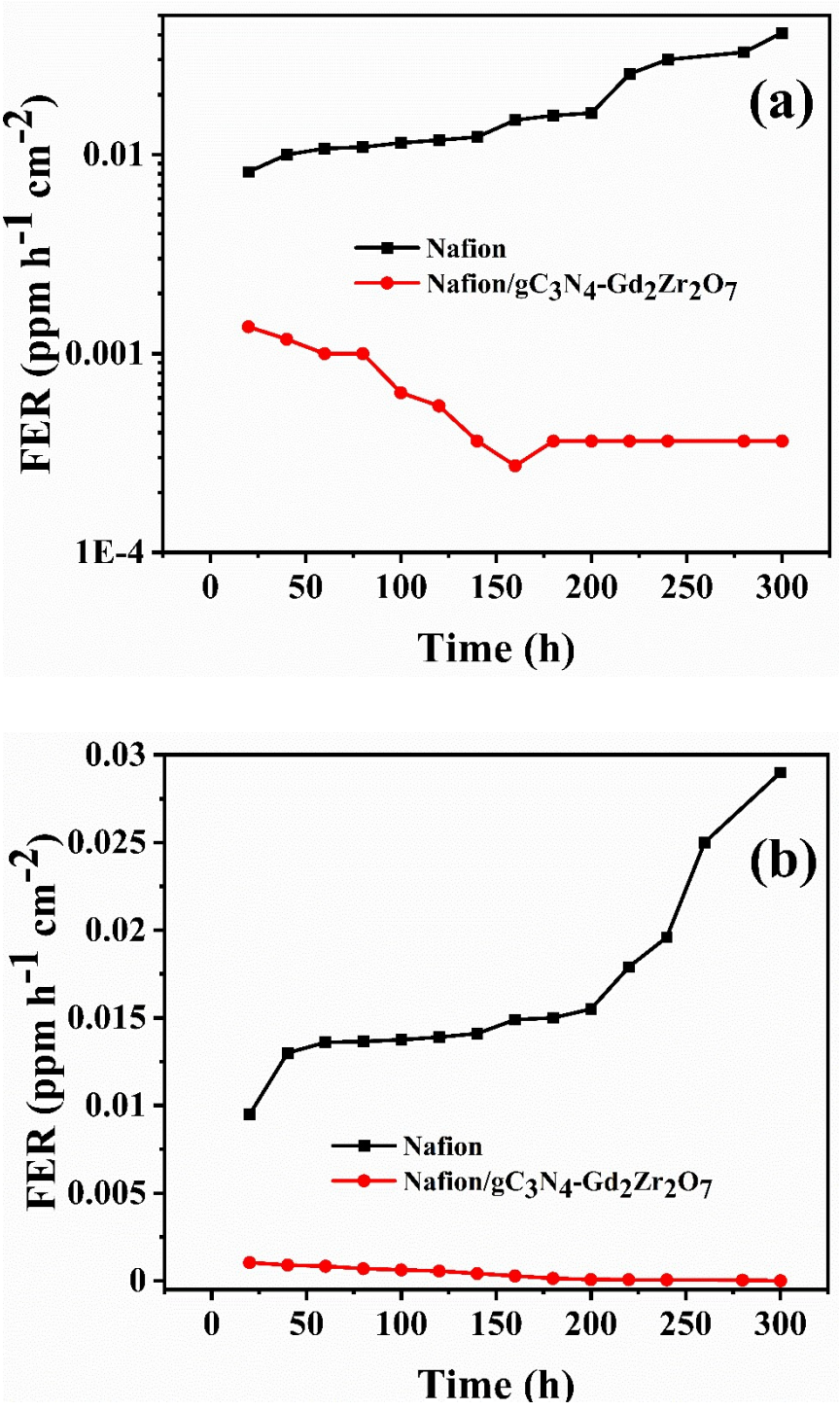

Fig. S14. Fluoride emission rate (FER) values measured during OCV holding test of pristine Nafion and Nafion/gC_3N_4-$Gd_2Zr_2O_7$ composite membranes at 100 °C under 30% RH at (a) anode and (b) cathode outlets.

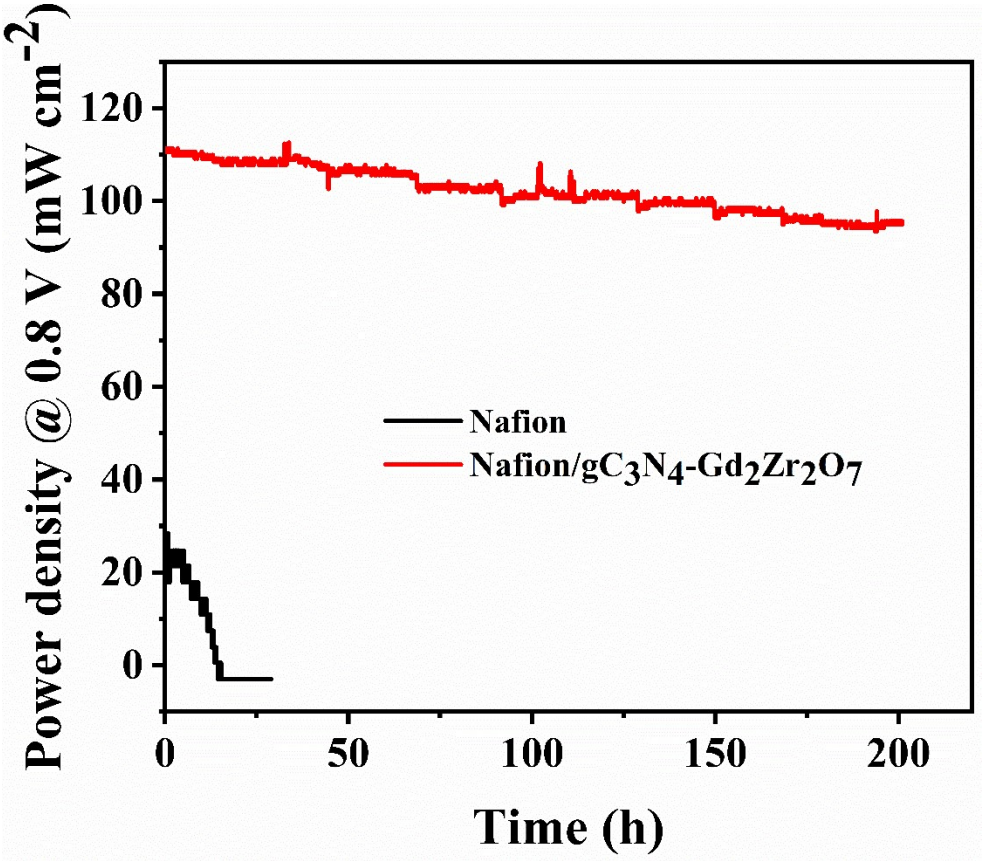

Fig. S15. Time-dependent power density of pristine Nafion and its composite membrane quantified at 100 °C under 30% RH by applying 0.8 V load.

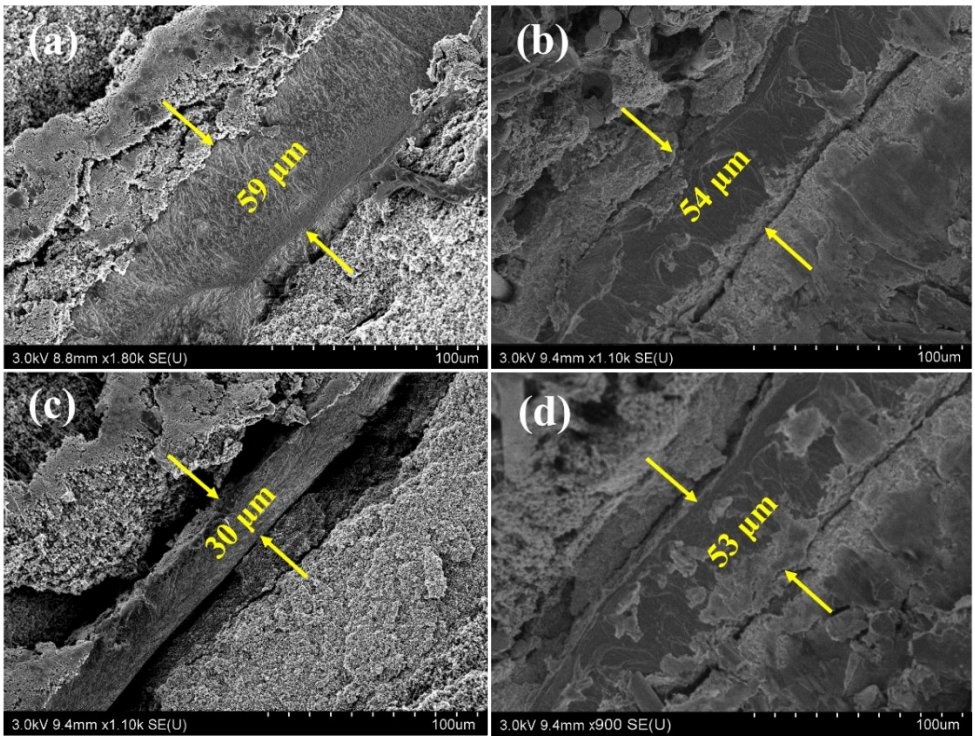

Fig. S16. SEM images of MEAs before and after OCV durability test at 100°C under 30% RH: (a and c) pristine Nafion and (b and d) Nafion/gC_3N_4-$Gd_2Zr_2O_7$.

Table S1. Water uptake, dimensional change, thickness change, ion exchange capacity (IEC), hydration number, and oxidative stability of Nafion-212, pristine Nafion, and composite membranes.

S. No	Membrane types	Water uptake (%)	Dimensional change (%)	Thickness change (%)	IEC (meq. g^{-1})	Hydration number (λ)	Oxidative stability (%)
1	Pristine Nafion	24.1	18.3	12.4	0.96	13.8	95.4
2	Nafion/gC_3N_4-$Gd_2Zr_2O_7$ (0.5 wt%)	27.6	16.2	17.3	0.94	16.2	96.8
3	Nafion/gC_3N_4-$Gd_2Zr_2O_7$ (1 wt%)	33.2	11.4	21.1	0.91	20.2	99.7
4	Nafion/gC_3N_4-$Gd_2Zr_2O_7$ (1.5 wt%)	35.6	10.1	22.6	0.90	21.3	100
5	Nafion-212	26.3	19.2	13.2	0.97	15.0	98.2

Table S2. Proton conductivity of Nafion -212, pristine Nafion and composite membranes with different wt% gC_3N_4-$Gd_2Zr_2O_7$.

S. No	Membrane types	Proton conductivity at 80 ˚C under 100% RH (mS cm^{-1})	Proton conductivity at 100 ˚C under 30% RH (mS cm^{-1})	Proton conductivity 120 ˚C under 15% RH (mS cm^{-1})
1	Pristine Nafion	140.7	11.0	2.3
2	Nafion/gC_3N_4-$Gd_2Zr_2O_7$ (0.5 wt%)	144.4	68.3	24.4
3	Nafion/ gC_3N_4-$Gd_2Zr_2O_7$ (1 wt%)	150.2	84.1	37.2
4	Nafion/ gC_3N_4-$Gd_2Zr_2O_7$ (1.5 wt%)	146.2	78.2	27.6
5	Nafion-212	145.1	19.3	3.3

Table S3. Comparison of proton conductivities of various Nafion-based membranes over 100 °C from recent literatures.

S. No	Membrane materials	Proton conductivity (mS cm^{-1})	Operating conditions		Ref.
			Temperature (˚C)	Relative humidity (%)	
1	Nafion/s-WR	~17	110	20	2019[12]
2	Nafion/silica	~13	110	20	2020[13]
3	Nafion/SO_3H-UGNF	127	120	50	2021[3]
4	Nafion/SO_3H-UGNF	10.1	120	18	2021[3]
5	Nafion/PTFE	~15	100	NA	2021[14]
6	Nafion/PTFE	~3	120	NA	2021[14]
7	Nafion/PTFE	~158	110	100	2021[15]
8	Nafion/PWA/Si	15	110	20	2021[16]
9	Nafion/gC_3N_4-$Gd_2Zr_2O_7$	84	100	30	This work
10	Nafion/gC_3N_4-$Gd_2Zr_2O_7$	37	125	15	This work

Table S4. Comparison of HFR of various Nafion-based membranes with present work.

S. No	Membrane types	HFR (m Ohm cm^{-2})	Operating conditions: Temperature (ºC) /RH (%)	References
1	Nafion-SSA	~790	80/25	[10]
2	Nafion-TNT	380	80/18	[11]
3	SnP_2O_7/Nafion	110	200/NA	[17]
4	GO-Nafion	~123	100/NA	[18]
5	Nafion/gC_3N_4-$Gd_2Zr_2O_7$	113	100/30	This work
6	Nafion-212	424	100/30	This work
7	Nafion/gC_3N_4-$Gd_2Zr_2O_7$	188	125/15	This work
8	Nafion-212	847	125/15	This work

References

1. M. Vinothkannan, R. Hariprasad, S. Ramakrishnan, A. R. Kim and D. J. Yoo, *ACS Sustainable Chemistry & Engineering*, 2019, **7**, 12847-12857.
2. D. Han, S. I. Hossain, B. Son, D. H. Lee and S. Shanmugam, *ACS Sustainable Chemistry & Engineering*, 2019, **7**, 16889-16899.
3. M. Vinothkannan, A. R. Kim, S. Ramakrishnan, Y.-T. Yu and D. J. Yoo, *Composites Part B: Engineering*, 2021, **215**, 108828.
4. S. Gahlot and V. Kulshrestha, *ACS Applied Materials & Interfaces*, 2015, **7**, 264-272.
5. S. Gahlot, P. P. Sharma, V. Kulshrestha and P. K. Jha, *ACS Applied Materials & Interfaces*, 2014, **6**, 5595-5601.
6. A. R. Kim, C. J. Park, M. Vinothkannan and D. J. Yoo, *Composites Part B: Engineering*, 2018, **155**, 272-281.
7. A. R. Kim, M. Vinothkannan and D. J. Yoo, *Journal of Energy Chemistry*, 2018, **27**, 1247-1260.
8. H. Zarrin, D. Higgins, Y. Jun, Z. Chen and M. Fowler, *The Journal of Physical Chemistry C*, 2011, **115**, 20774-20781.
9. C. Xu, Y. Cao, R. Kumar, X. Wu, X. Wang and K. Scott, *Journal of Materials Chemistry*, 2011, **21**, 11359-11364.
10. K. Oh, O. Kwon, B. Son, D. H. Lee and S. Shanmugam, *Journal of Membrane Science*, 2019, **583**, 103-109.
11. K. Ketpang, K. Lee and S. Shanmugam, *ACS Applied Materials & Interfaces*, 2014, **6**, 16734-16744.
12. G. Xu, Z. Wei, S. Li, J. Li, Z. Yang and S. A. Grigoriev, *International Journal of Hydrogen Energy*, 2019, **44**, 29711-29716.
13. G. Xu, Z. Wu, Z. Wei, W. Zhang, J. Wu, Y. Li, J. Li, K. Qu and W. Cai, *Renewable Energy*, 2020, **153**, 935-939.
14. X. Zhang, D. Trieu, D. Zheng, W. Ji, H. Qu, T. Ding, D. Qiu and D. Qu, *Industrial & Engineering Chemistry Research*, 2021, **60**, 11086-11094.
15. S. Ryu, B. Lee, J.-H. Kim, C. Pak and S.-H. Moon, *International Journal of Energy Research*, 2021, **45**, 19136-19146.
16. G. Xu, S. Xue, Z. Wei, J. Li, K. Qu, Y. Li and W. Cai, *International Journal of Hydrogen Energy*, 2021, **46**, 4301-4308.
17. K. P. Ramaiyan, S. Herrera, M. J. Workman, T. A. Semelsberger, V. Atanasov, J. Kerres, S. Maurya, Y. S. Kim, C. R. Kreller and R. Mukundan, *Journal of Materials Chemistry A*, 2020, **8**, 16345-16354.
18. A. Ibrahim, O. Hossain, J. Chaggar, R. Steinberger-Wilckens and A. El-Kharouf, *International Journal of Hydrogen Energy*, 2020, **45**, 5526-5534.